

Notch fracture toughness of glasses: Rate, age and geometry dependence

Manish Vasoya¹, Chris H. Rycroft^{2,3} and Eran Bouchbinder¹

¹ *Chemical Physics Department, Weizmann Institute of Science, Rehovot 7610001, Israel*

² *Paulson School of Engineering and Applied Sciences,
Harvard University, Cambridge, MA 02138, United States*

³ *Department of Mathematics, Lawrence Berkeley Laboratory, Berkeley, California 94720, United States*

Understanding the fracture toughness (resistance) of glasses is a fundamental problem of prime theoretical and practical importance. Here we theoretically study its dependence on the loading rate, the age (history) of the glass and the notch radius ρ . Reduced-dimensionality analysis suggests that the notch fracture toughness results from a competition between the initial, age- and history-dependent, plastic relaxation timescale τ_0^{pl} and an effective loading timescale $\tau^{ext}(K_I, \rho)$, where K_I is the tensile stress-intensity-factor rate. The toughness is predicted to scale with $\sqrt{\rho}$ independently of $\xi \equiv \tau^{ext}/\tau_0^{pl}$ for $\xi \ll 1$, to scale as $T\sqrt{\rho} \log(\xi)$ for $\xi \gg 1$ (related to thermal activation, where T is the temperature) and to feature a non-monotonic behavior in the crossover region $\xi \sim \mathcal{O}(1)$ (related to plastic yielding dynamics). These predictions are verified using novel 2D computations, providing a unified picture of the notch fracture toughness of glasses. The theory highlights the importance of timescales competition and far from steady-state elasto-viscoplastic dynamics for understanding the toughness, and shows that the latter varies quite significantly with the glass age (history) and applied loading rate. Experimental support for bulk metallic glasses is presented.

I. INTRODUCTION

The fracture toughness, i.e. the ability to resist failure in the presence of a crack, is a basic physical property of materials [1]. From a practical perspective, this property is a major limiting factor in the structural integrity of a broad range of systems. From a theoretical perspective, the fracture toughness challenges our understanding of the strongly nonlinear and dissipative response of materials under extreme conditions, approaching catastrophic failure. Consequently, obtaining a basic understanding of the fracture toughness of materials is a fundamentally important problem.

Quantitatively predicting the fracture toughness of glassy materials, which lack long-range crystalline order and are characterized by intrinsic disorder, is a particularly pressing problem. Glassy materials exhibit unique and intriguing physical properties as compared to their crystalline counterparts [2–9]. For example, glassy solids typically exhibit a strength and an elastic limit that significantly exceed those of crystalline alloys of similar composition due to the absence of mobile dislocation defects. Instead, glassy solids deform irreversibly by immobile and localized structural rearrangements [10–12], at sites termed Shear-Transformation-Zones (STZ), which are not yet fully understood.

Glassy materials are intrinsically out-of-equilibrium, hence their physical properties depend on their history and age (see, for example, [13, 14]). Moreover, these materials typically do not feature strain-hardening, i.e. an increase in the deformation resistance with increasing deformation, which is commonly observed in crystalline alloys [2–9]. Finally, glassy materials also feature rate effects that are far from understood [2–9].

In the last few decades significant progress has been made in using conventional casting techniques to obtain multi-component amorphous alloys in bulk forms, the so-

called Bulk Metallic Glasses (BMG) [15–20]. The emergence of this new family of glasses, which possess superior properties, has triggered intense research activity and holds a great promise for a wide range of engineering applications [2–9]. The fracture toughness of these materials, though, still raises serious concerns and hence the current usage of BMG in structural applications is limited.

Consequently, the fracture toughness of glasses, and of BMG in particular, has been the subject of various recent studies [21–47]. Yet, there is no complete understanding of the resistance of glassy materials to catastrophic failure in the presence of a notch defect — the notch fracture toughness — and its dependence on various physical parameters. Our goal in this paper is to offer a comprehensive theoretical picture of the dependence of the notch fracture toughness of glasses on the loading rate, the glass age/history, the notch radius and the temperature (below the glass transition temperature).

Our main result, obtained through a reduced-dimensionality theoretical analysis and extensive 2D spatiotemporal computations based on a novel numerical method [48], highlights the essential role played by timescales competition in determining the notch fracture toughness of glassy materials. The competing timescales involve an effective applied loading timescale (depending on the notch radius of curvature, and on the global geometry and loading rate) and the initial, age-dependent, plastic (dissipative) relaxation timescale (depending on the glass age and history) [49]. Once properly identified, the ratio of the two timescales is shown to control the fracture toughness over a wide range of physical conditions. The dependence of the toughness on the dimensionless timescale ratio is quantitatively derived and is shown to feature a *non-monotonic* behavior. Our results are shown to be consistent with existing experimental data and offer various new predictions.

II. PROBLEM FORMULATION

The fracture toughness quantifies the amount of dissipation involved in crack propagation. Consequently, one needs to account for the irreversible deformation of the material, and its interplay with reversible (elastic) deformation. Inertia plays little role in fracture *initiation* under a wide range of conditions and standard engineering testing protocols, hence we focus on quasi-static stress equilibrium described by

$$\nabla \cdot \boldsymbol{\sigma} = \mathbf{0}, \quad (1)$$

where $\boldsymbol{\sigma}$ is the Cauchy stress tensor. We consider then a general hypo-elasto-viscoplastic material described by

$$\mathbf{D}^{tot}(\mathbf{v}) = \mathbf{D}^{el}(\boldsymbol{\sigma}, \mathbf{v}) + \mathbf{D}^{pl}(\boldsymbol{\sigma}, \dots). \quad (2)$$

Here $\mathbf{D}^{tot} = \frac{1}{2}[\nabla \mathbf{v} + (\nabla \mathbf{v})^T]$ is the total rate of deformation tensor, where $\mathbf{v}(\mathbf{r}, t)$ is the Eulerian velocity field and (\mathbf{r}, t) are the spatiotemporal coordinates. $\mathbf{D}^{el} = \partial_t \boldsymbol{\epsilon} + \mathbf{v} \cdot \nabla \boldsymbol{\epsilon} + \boldsymbol{\epsilon} \cdot \boldsymbol{\omega} - \boldsymbol{\omega} \cdot \boldsymbol{\epsilon}$ is the elastic rate of deformation tensor, where $\boldsymbol{\omega} = \frac{1}{2}[\nabla \mathbf{v} - (\nabla \mathbf{v})^T]$ is the spin tensor and the strain tensor $\boldsymbol{\epsilon}$ is related to $\boldsymbol{\sigma}$ through Hooke's law $\boldsymbol{\sigma} = K \text{tr} \boldsymbol{\epsilon} \mathbf{1} + 2\mu (\boldsymbol{\epsilon} - \frac{1}{3} \text{tr} \boldsymbol{\epsilon} \mathbf{1})$. K and μ are the bulk and shear moduli, respectively. $\mathbf{D}^{pl}(\boldsymbol{\sigma}, \dots)$ is the plastic rate of deformation tensor, which encapsulates the relevant physics of the dissipative deformation of glasses. The ellipsis stands for additional dependencies, e.g. on the temperature and on structural internal state variables.

We adopt the non-equilibrium thermodynamic Shear-Transformation-Zones (STZ) model, as in [33], where

$$\mathbf{D}^{pl}(\mathbf{s}, T, \chi) = e^{-\frac{e_z}{k_B \chi}} \frac{\mathcal{C}(\bar{s}, T)}{\tau} \left[1 - \frac{s_y}{\bar{s}} \right] \frac{\mathbf{s}}{\bar{s}}, \quad (3)$$

$$c_0 \dot{\chi} = \frac{\mathbf{D}^{pl} : \mathbf{s}}{s_y} (\chi_\infty - \chi), \quad (4)$$

for $\bar{s} \geq s_y$ and $\mathbf{D}^{pl} = 0$ otherwise. This model, despite its relative simplicity, has been shown to capture a wide range of driven glassy phenomena [12, 33, 50–63]. $\mathbf{s} = \boldsymbol{\sigma} - \frac{1}{3} \text{tr} \boldsymbol{\sigma} \mathbf{1}$ in Eqs. (3)-(4) is the deviatoric stress tensor, its magnitude is $\bar{s} \equiv \sqrt{\mathbf{s} : \mathbf{s} / 2}$, and s_y is the shear yield stress. χ is an effective disorder temperature which quantifies the intrinsic structural state of the glass [50, 56], e_z/k_B is a typical STZ formation energy over Boltzmann's constant, $\mathcal{C}(\bar{s}, T)/\tau$ is the rate at which STZ make transitions between their internal states. τ^{-1} is a molecular vibration rate and T is the bath temperature, assumed to be well below the glass temperature (such that spontaneous aging is neglected in Eq. (4)). c_0 is an effective dimensionless heat capacity and χ_∞ is the steady state value of χ .

The STZ transition rate is taken to be of the form

$$\mathcal{C}(\bar{s}, T) = \begin{cases} e^{-\frac{\Delta}{k_B T}} \cosh \left[\frac{\Omega \epsilon_0 \bar{s}}{k_B T} \right] & \text{for } \Omega \epsilon_0 \bar{s} < \Delta \\ \frac{\Omega \epsilon_0 \bar{s}}{2\Delta} & \text{for } \Omega \epsilon_0 \bar{s} \geq \Delta. \end{cases} \quad (5)$$

It corresponds to a linearly stress-biased thermal activation process at relatively small stresses, where Δ is the

typical energy activation barrier, Ω is the typical activation volume and ϵ_0 is the typical local STZ strain. In the presence of the high stresses near a tip of a crack, $\Omega \epsilon_0 \bar{s}$ may become larger than Δ , in which case we assume that the exponential thermal activation form crosses over to a much weaker dependence associated with a linear, non-activated, dissipative mechanism [54]. As $\Delta \gg k_B T$, the two regimes connect continuously, but not differentiably. This crossover in the form of the STZ transition rates, from exponential thermal activation to a much weaker athermal power-law (here a linear relation, which allows for analytic progress), will turn out below to have important implications for the toughness.

This elasto-viscoplasticity model is used to formulate a plane-strain fracture problem where traction-free boundary conditions are imposed on a blunted straight notch (crack) with an initial root radius ρ (cf. Fig. 1) and the universal linear elastic mode I (tensile) crack tip velocity fields [64]

$$\mathbf{v}(r, \theta, t) = \frac{\dot{K}_I(t)}{\mu} \sqrt{\frac{r}{2\pi}} \mathbf{F}(\theta) \quad \text{for } r \gg \rho \quad (6)$$

are imposed on a scale much larger than ρ . Here \dot{K}_I is the mode I stress-intensity-factor rate, which measures the intensity of the linear elastic singularity $\nabla \mathbf{v} \sim 1/\sqrt{2\pi r}$ at $\rho \ll r \ll L$, where L is a macroscopic lengthscale in the global fracture problem (e.g. the sample size). (r, θ) is a polar coordinate system whose origin is set a distance $\rho/5$ behind the notch root, $\theta = 0$ is the symmetry axis and $\mathbf{F}(\theta)$ is a known universal function [33, 64]. In such a boundary layer formulation, the stress-intensity-factor uniquely couples the inner scales near the notch root to the outer scales, and hence can be controlled independently without solving the global fracture problem [64].

The fracture toughness is the critical value of the stress-intensity-factor, K_{Ic} , at which crack propagation initiates and global failure occurs. Recent work [33, 38–47] suggests that this onset (and in fact also the subsequent propagation [33]) is controlled by a local cavitation instability occurring when the hydrostatic tension $\frac{1}{3} \text{tr} \boldsymbol{\sigma}$ surpasses a threshold level σ_c . We adopt this failure criterion here.

While a large part of the analysis below is performed in terms of dimensionless parameters, we nevertheless consider realistic material parameters corresponding to Vitreloy 1, a widely studied BMG, identical to those reported in [33]. That is, we use: $T = 400$ K, $e_z/k_B = 21000$ K, $s_y = 0.85$ GPa, $\mu = 37$ GPa, $K = 122$ GPa, $\tau = 10^{-13}$ s, $\epsilon_0 = 0.3$, $\Omega = 300 \text{ \AA}^3$, $c_0 = 0.4$, $\Delta/k_B = 8000$ K and $\chi_\infty = 900$ K. For the initial conditions we use $\boldsymbol{\sigma}(\mathbf{r}, t=0) = 0$ and $\chi(\mathbf{r}, t=0) = \chi_0$, where χ_0 describes the initial structural state of the glass which depends on its history. For example, it may be affected by the cooling rate at which the glass has been formed, annealing and other heat treatments, aging time and previous deformation. The model's setup is shown in Fig. 1.

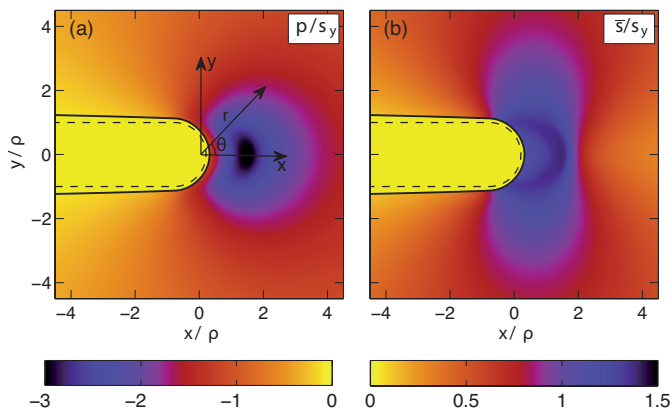


FIG. 1. (Color online) The problem setting and an example of a numerical solution in the near notch root region. (a) The hydrostatic pressure and (b) the magnitude of the deviatoric stress, both normalized by the shear yield stress s_y , are shown. The dashed-dotted line corresponds to the initial notch state and the solid line to a deformed state with $K_I = 30 \text{ MPa}\sqrt{\text{m}}$. A small portion of the simulation domain $-20 \leq x/\rho, y/\rho \leq 20$, near the notch root, is shown. A fixed coordinate system located a distance $\rho/5$ behind the initial notch root, with both Cartesian (x, y) and polar (r, θ) coordinates, is shown on panel (a). The calculation was done using a 1025×1025 grid.

III. THEORY AND ANALYSIS

Our major goal is to study the dependence of the fracture toughness K_{Ic} on the structural state of the glass χ_0 , on the stress-intensity-factor rate \dot{K}_I , on the notch radius of curvature ρ and on the temperature T below the glass transition temperature. We address the problem of calculating $K_{Ic}(\chi_0, \dot{K}_I, \rho, T)$ by a reduced-dimensionality theoretical analysis and 2D numerical computations. The latter, an example of which is shown in Fig. 1, are based on a recently developed numerical method that can handle physically realistic loading rates, which is essential for understanding the properties of the toughness. Preliminary numerical results addressing this problem appeared in [33].

To gain some analytic insight into the fracture toughness, we perform a reduced-dimensionality analysis which aims at describing the behavior of a representative material element near the notch root. We further simplify the problem by eliminating its tensorial nature, focusing only on the magnitude of the deviatoric component of the relevant tensors. In particular, we neglect altogether the hydrostatic part of the stress tensor $\boldsymbol{\sigma}$ and replace its deviatoric part $\mathbf{s}(\mathbf{r}, t)$ by a space-independent scalar $s(t)$, and $\chi(\mathbf{r}, t)$ by $\chi(t)$. Similarly, we replace the space-dependent elastic and plastic rate of deformation tensors in the problem by their space-independent scalar counterparts $\mathbf{D}^{el}(\mathbf{r}, t) \rightarrow \dot{s}(t)/\mu$ and $\mathbf{D}^{pl}(\mathbf{r}, t) \rightarrow D^{pl}(t)$, with $D^{pl}(s, \chi) = \tau^{-1} e^{-\frac{e_z}{k_B \chi}} \mathcal{C}(s, T) (1 - s_y/s)$.

The crucial last step is to relate the global loading and

geometry of the system, captured by the stress-intensity-factor K_I , and the effective total rate of the deformation near the notch root, taking into account both the strong stress amplification associated with the linear elastic square root singularity and the characteristic length-scale inherited from the notch radius of curvature. A natural way to do this is through the replacement

$$\mathbf{D}^{tot}(\mathbf{r}, t) \rightarrow \frac{\dot{K}_I}{\mu\sqrt{2\pi\rho}}. \quad (7)$$

With these replacements, Eqs. (3)-(4) transform into a set of coupled nonlinear ordinary differential equations

$$\dot{s} = \frac{\dot{K}_I}{\sqrt{2\pi\rho}} - \mu D^{pl}(s, \chi), \quad (8)$$

$$c_0 \dot{\chi} = \frac{D^{pl}(s, \chi) s}{s_y} (\chi_\infty - \chi). \quad (9)$$

Obviously, Eqs. (8)-(9) miss many features of the full 2+1 dimensional spatiotemporal dynamics of the problem, such as the tensorial nature of the basic quantities, the coupling between the deviatoric and hydrostatic parts of the deformation/stress, the time evolution of the radius of curvature $\rho(t)$ and the propagation of yielding fronts in the notch root region. Yet, as will be shown below, they capture important aspects of the fracture toughness. The first step in analyzing Eqs. (8)-(9) is to identify a proper set of dimensionless physical parameters that control their behavior. In this context, we stress that elasto-viscoplasticity is intrinsically linked to a competition between different timescales. Moreover, glassy response is sensitive to the *initial* structural state of the material (affected by its age, cooling rate, previous deformation, etc.), which must play a crucial role in far from steady-state physical properties such as the fracture toughness.

To capture this timescale competition, we define an *initial* plastic relaxation timescale (inverse rate) as $\tau_0^{pl}(\chi_0) \equiv \tau e^{\frac{e_z}{k_B \chi_0}}$, an effective applied timescale (again, an inverse rate) as $\tau^{ext}(\dot{K}_I, \rho) \equiv \mu\sqrt{2\pi\rho}/\dot{K}_I$ and their ratio

$$\xi(\chi_0, \dot{K}_I, \rho) \equiv \frac{\tau^{ext}}{\tau_0^{pl}} = \frac{\mu\sqrt{2\pi\rho}}{\tau\dot{K}_I} e^{-\frac{e_z}{k_B \chi_0}}. \quad (10)$$

This dimensionless quantity plays a central role in what follows. It is important to note that $1/\tau^{ext}$ is *not* the externally applied strain-rate, but rather the effective strain-rate experienced by the near notch region. The effective strain-rate at the innermost scale $r \simeq \rho$ is significantly amplified relative to the externally applied strain-rate, characterizing the outermost scale L , according to the linear elastic square root singularity.

We also define $\tilde{e}_z \equiv e_z/k_B \chi_0$, $\tilde{\chi}_\infty \equiv \chi_\infty/\chi_0$, $\tilde{\mu} \equiv \mu c_0/s_y$, $\tilde{s} \equiv s/s_y$, $\tilde{\chi} \equiv \chi/\chi_0$ and $\tilde{t} \equiv t\dot{K}_I/s_y\sqrt{2\pi\rho}$. In terms of these dimensionless quantities, Eqs. (8)-(9) take the form

$$\dot{\tilde{s}} = 1 - \xi f(\tilde{s}, \tilde{\chi}), \quad (11)$$

$$\tilde{\mu} \dot{\tilde{\chi}} = \xi f(\tilde{s}, \tilde{\chi}) \tilde{s} (\tilde{\chi}_\infty - \tilde{\chi}), \quad (12)$$

with $f(\tilde{s}, \tilde{\chi}) \equiv e^{\tilde{e}_z(1-\tilde{\chi}^{-1})}\mathcal{C}(s, T)(1 - \tilde{s}^{-1})$ for $\tilde{s} \geq 1$ (for $\tilde{s} < 1$ we have $f=0$). It should be noted that nondimensionalizing differential equations using an initial condition, in our case χ_0 , might appear unnatural. Yet, it is a choice that is dictated by the physics of glasses, which exhibit a rather unique dependence on the initial state.

To proceed, we distinguish between two regimes, one in which the deviatoric stress significantly surpasses $\Delta/\Omega \epsilon_0$, where $\mathcal{C} \sim s$, and one in which the deviatoric stress remains close to $\Delta/\Omega \epsilon_0$, where \mathcal{C} varies exponentially with the stress (cf. Eq. (5)). We focus first on the former and for the sake of simplicity set $2\Delta/\Omega \epsilon_0 = s_y$, which means that we exclude thermal activation altogether in this part of the reduced-dimensionality analysis.

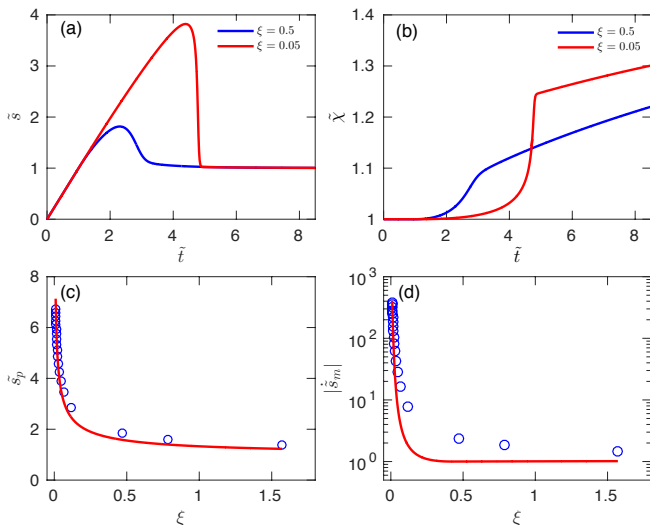


FIG. 2. (Color online) The solution of Eqs. (11)-(12), for two values of ξ (separated by an order of magnitude). The stress is shown in panel (a) and the effective temperature in panel (b). We used $\tilde{\mu} = 15.07$, $\tilde{e}_z = 35$, $\tilde{\chi}_\infty = 1.5$ and $\mathcal{C} = \tilde{s}$, with the initial conditions $\tilde{s}(0) = 0$ and $\tilde{\chi}(0) = 1$. (c) The analytic prediction for the peak stress \tilde{s}_p in Eq. (13) (solid red line) compared to the peak stress obtained from a numerical solution of Eqs. (11)-(12) (open blue circles). (d) The prediction of the maximal stress drop rate $|\dot{\tilde{s}}_m|$ in the post-peak regime following Eq. (14) (solid red line) compared to the maximal stress drop rate obtained from a numerical solution of Eqs. (11)-(12) (open blue circles).

In Fig. 2a-b we present $\tilde{s}(\tilde{t})$ and $\tilde{\chi}(\tilde{t})$ for two values of ξ which differ by an order of magnitude. It is observed that as ξ decreases, when τ^{ext} decreases relative to τ_0^{pl} , the yielding behavior of the material (i.e. the transition from elastic-dominated to plastic-dominated deformation) changes quite significantly. In particular, an elastic overshoot leads to a significant increase in the peak stress \tilde{s}_p with decreasing ξ , and the subsequent dynamics exhibit a sharp drop in the stress \tilde{s} and a sharp increase in the effective temperature $\tilde{\chi}$. These sharp post-yielding dynamics mark the emergence of a short timescale associated with strongly nonlinear material response.

Our next goal is to better understand this behavior and its relation to the fracture toughness. To that aim, we first try to estimate the peak stress \tilde{s}_p , for which $\dot{\tilde{s}}=0$. The latter translates into the relation $e^{\tilde{e}_z(1-\tilde{\chi}_p^{-1})}(\tilde{s}_p - 1) = \xi^{-1}$ between \tilde{s}_p and $\tilde{\chi}_p \equiv \tilde{\chi}(\tilde{s}_p)$. An approximate solution for the stress peak can be derived in the form

$$\tilde{s}_p \simeq 1 - \frac{\zeta + \tilde{\mu}}{4\zeta} + \frac{\sqrt{8\zeta\tilde{\mu}\xi^{-1} + (\zeta + \tilde{\mu})^2}}{4\zeta}, \quad (13)$$

with $\zeta \equiv 1 + \tilde{e}_z(\tilde{\chi}_\infty - 1)$. $\tilde{\chi}_p$ is given by the exact relation $\tilde{\chi}_p(\tilde{s}_p) = (1 + \tilde{e}_z^{-1} \log[\xi(\tilde{s}_p - 1)])^{-1}$. In Fig. 2c we compare the analytic estimation in Eq. (13) to the peak stress obtained from the full numerical solution of Eqs. (8)-(9). It is observed that the analytic approximation accurately captures the increase in \tilde{s}_p with decreasing ξ . In light of the latter, we expect $\tilde{\chi}_p(\tilde{s}_p)$ given above to yield good approximations as well, which is indeed the case (not shown).

With \tilde{s}_p and $\tilde{\chi}_p$ at hand, we can estimate the stress drop rate in the post-peak dynamics, observed in Fig. 2a. As the plastic rate of deformation is strongly amplified during the drop, we neglect the external loading term $\dot{K}_I/\sqrt{2\pi\rho}$ in Eq. (8). With this approximation, we can eliminate $D^{pl}(s, \chi)$ between Eqs. (8)-(9), obtaining a differential equation for $\chi(s)$ (i.e. time becomes a parameter). The solution, which is expected to be valid deep inside the stress drop region, takes the form $\tilde{\chi}(\tilde{s}) \simeq \tilde{\chi}_\infty - (\tilde{\chi}_\infty - \tilde{\chi}_p) \exp\left(\frac{\tilde{s}^2 - \tilde{s}_p^2}{2\tilde{\mu}}\right)$. Using the latter, we obtain the following estimate

$$\dot{\tilde{s}}(\tilde{s}) \simeq -\xi e^{\tilde{e}_z[1-\tilde{\chi}(\tilde{s})^{-1}]}(\tilde{s} - 1) \quad (14)$$

for the stress rate during the drop, which should be valid for $1 < \tilde{s} < \tilde{s}_p$, not too close to either 1 or \tilde{s}_p .

It is important to note that $\tilde{\chi}(\tilde{s})$ in Eq. (14) depends on ξ also through \tilde{s}_p and $\tilde{\chi}_p(\tilde{s}_p)$, which give rise to a super-exponential increase in the maximal value of $\dot{\tilde{s}}(\tilde{s})$, $|\dot{\tilde{s}}_m|$, with decreasing ξ . The prediction in Eq. (14) is compared to the full solution in Fig. 2d, demonstrating reasonable agreement at small values of ξ . Note that $|\dot{\tilde{s}}_m|$ in Fig. 2d is one to two orders of magnitude larger than the effective external loading rate (which is unity in the dimensionless form, cf. Eq. (11)) for sufficiently small ξ , as assumed before. This analysis shows how nonlinear yielding in glassy materials can dynamically generate new, and much shorter, timescales.

In order to understand the implications of this reduced-dimensionality analysis on the toughness, we need to consider spatial interactions between different material elements and the coupling between the deviatoric and the hydrostatic components of the stress tensor. When a material element undergoes yielding dynamics, the stress will be redistributed to nearby material elements. In particular, when ξ is small and a sharp deviatoric stress drop as shown in Fig. 2a emerges, nearby material elements will experience a *sharp increase* in stress. This applies to

both the deviatoric \mathbf{s} and the hydrostatic $\frac{1}{3}\text{tr}\boldsymbol{\sigma}$ components of the stress tensor $\boldsymbol{\sigma}$, which are coupled through the stress equilibrium equation $\nabla \cdot \boldsymbol{\sigma} = 0$. To show this, we plot in Fig. 3a the maximum (in space) of the magnitude of the deviatoric stress \mathbf{s} , \bar{s}_m , and of the hydrostatic tension $\frac{1}{3}\text{tr}\boldsymbol{\sigma} \equiv -p$, $|p|_m$, obtained from a numerical solution of the full 2+1 dimensional problem with $\chi_0 = 595$ K and $\dot{K}_I = 25$ MPa $\sqrt{\text{m}}$ /s (corresponding to $\xi = 0.14$). We observe that indeed both quantities abruptly increase *together* at a certain applied stress-intensity-factor K_I .

If the increase in $|p|_m$ for the given ξ is sufficiently large, it can reach the threshold σ_c , which in our model implies failure (and hence the toughness is determined). Consider then what happens for yet smaller values of ξ , $\xi \ll 1$, corresponding to larger \dot{K}_I 's or smaller χ_0 's. In this case, we expect the threshold σ_c to be reached within the predominantly elastic regime and hence the toughness to be ξ -independent in this regime. This implies that there might be a range of ξ 's in which the toughness decreases when ξ increases. That is, this scenario implies that the toughness can vary *non-monotonically* with ξ . To test this, we plot in Fig. 3b $|p|_m$ for $\xi = 0.14$ (exactly the as in Fig. 3a) and also for $\xi = 4 \times 10^{-3} \ll 1$, along with $\sigma_c = 4.5s_y$ (horizontal line, the same value as in [33]). We indeed observe that the threshold is reached at a smaller K_I for the larger ξ , i.e. that the fracture toughness is indeed non-monotonic.

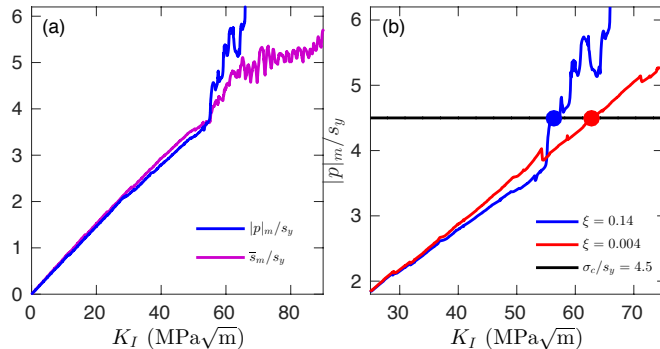


FIG. 3. (Color online) (a) The maximum (in space) of the hydrostatic tension $|p|_m$ and the magnitude of the deviatoric stress \bar{s} (both in units of s_y) as a function of K_I , obtained from a numerical solution of the full 2+1 dimensional problem with $\chi_0 = 595$ K, $\dot{K}_I = 25$ MPa $\sqrt{\text{m}}$ /s and $\rho = 65$ μm , corresponding to $\xi = 0.14$. It is observed that the two quantities experience an abrupt increase at the same value of K_I . (b) The maximum (in space) of the hydrostatic tension $|p|_m$ (in units of s_y) as a function of K_I , for $\xi = 0.14$ (as in panel (a)) and $\xi = 4 \times 10^{-3} \ll 1$, together with a cavitation threshold corresponding to $\sigma_c/s_y = 4.5$ (solid black horizontal line). It is observed that for the larger ξ , the cavitation threshold is exceeded at a smaller K_I , implying a non-monotonic behavior of the fracture toughness.

These predictions are tested over a wide range of parameters in Fig. 4a-b, where we plot the toughness as a function of \dot{K}_I (panel (a)), for various χ_0 's and χ_0 (panel (b)), for various \dot{K}_I 's, as obtained from the full

2+1 dimensional computations. The emergence of a non-monotonic dependence of the toughness for a large range of parameters is evident, as well as the saturation of the toughness for sufficiently small χ_0 and sufficiently large \dot{K}_I (corresponding to $\xi \ll 1$). The minimum in the toughness shifts systematically with χ_0 and \dot{K}_I . Note that while the non-monotonicity is not huge in magnitude, of the order of 10 MPa $\sqrt{\text{m}}$, it is a distinct and qualitative feature of strongly nonlinear yielding dynamics in our model. Note also that the non-monotonic behavior disappears for large enough χ_0 (cf. the $\chi_0 = 640$ K curve on panel (a)) and large enough \dot{K}_I (not shown on panel (b), it requires yet larger \dot{K}_I values).

Finally, we also plot in Fig. 4c the variation of the toughness with ρ (for various χ_0 's, with $\dot{K}_I = 20$ MPa $\sqrt{\text{m}}$ /s), to be discussed below. The toughness is obviously a monotonically increasing function of ρ , as increasing the notch radius of curvature implies enhanced plastic dissipation and less stress concentration. Yet the monotonic ρ dependence in panel (c) will be connected below to the non-monotonic behavior observed in panels (a)-(b) with respect to χ_0 and \dot{K}_I .

IV. THE MAIN RESULT

Up to now, in the analysis of the reduced-dimensionality model in Eqs. (8)-(9) we used $\mathcal{C} \sim s$. This cannot be valid in the large χ_0 and small \dot{K}_I limits (corresponding to large ξ), where stresses remain close to s_y and $\mathcal{C}(\cdot)$ in Eq. (5) is expected to be determined by thermal activation. Consequently, we would like now to gain some insight into the behavior of Eqs. (8)-(9) when $\mathcal{C}(s, T) = e^{-\Delta/k_B T} \cosh[\Omega \epsilon_0 s/k_B T]$. As the stress remains close to s_y , we assume that $\chi \simeq \chi_0$ and expand $\dot{s} = 0$ near s_y . We can then solve for the peak stress, which takes the form $\tilde{s}_p = 1 + \psi^{-1} W(2\psi \xi^{-1} e^{\Delta/k_B T} e^{-\psi})$, where $\psi \equiv \frac{\Omega \epsilon_0 s_y}{k_B T}$ and $W(\cdot)$ is the Lambert W-function. For realistic numbers, the argument of the latter is large and we have $W(x) \simeq \log(x)$. Consequently, \tilde{s}_p depends on ξ through $T \log \xi$, a clear signature of thermal activation. We *hypothesize* that the toughness K_{Ic} features the same dependence when ξ is large, i.e. when stresses remain relatively small.

We are now ready to put all elements of the analysis into a unified prediction for $K_{Ic}(\chi_0, \dot{K}_I, \rho, T)$. The analysis above suggests that the natural quantity to consider is actually $K_{Ic}/\sqrt{\rho}$ (which can be made dimensionless using a stress scale, say s_y). Consequently, we have

$$\frac{K_{Ic}(\chi_0, \dot{K}_I, \rho, T)}{\sqrt{\rho}} \sim \begin{cases} \text{Const.} & \text{for } \xi \ll 1 \\ g(\xi) & \text{for } \xi \sim \mathcal{O}(1) \\ T \log(\xi) & \text{for } \xi \gg 1, \end{cases} \quad (15)$$

where $g(\xi)$ features a non-monotonic behavior for not too large χ_0 and \dot{K}_I (i.e. $g(\xi)$ is not a unique function of ξ for large enough χ_0 and \dot{K}_I). To test this major

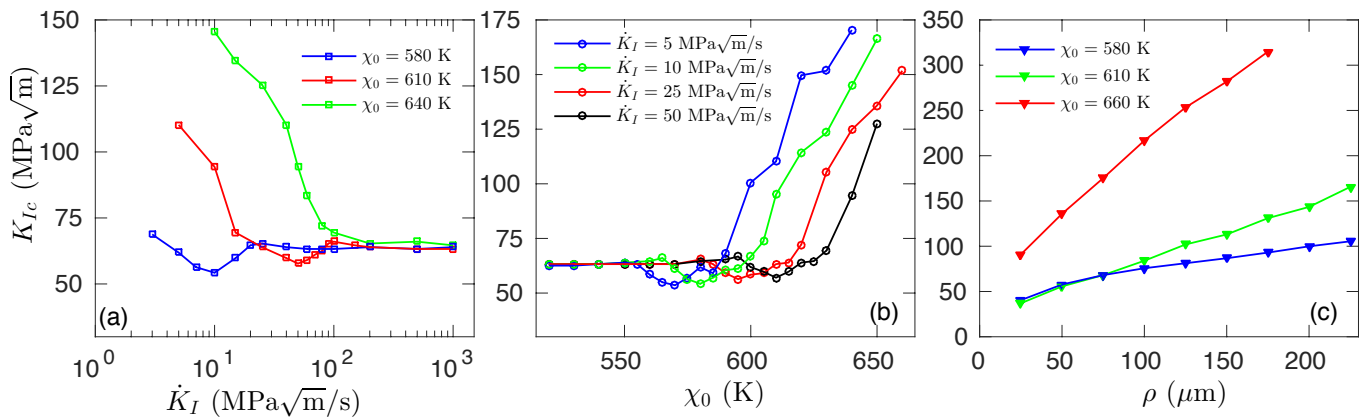


FIG. 4. (Color online) The notch fracture toughness $K_{Ic}(\chi_0, \dot{K}_I, \rho, T)$ as obtained from numerical solutions of the full 2+1 dimensional problem. (a) K_{Ic} as a function of \dot{K}_I for various χ_0 's, with $\rho = 65 \mu\text{m}$ and $T = 400 \text{ K}$. (b) K_{Ic} as a function of the initial structural state χ_0 for various \dot{K}_I 's, with $\rho = 65 \mu\text{m}$ and $T = 400 \text{ K}$. (c) K_{Ic} as a function of the notch radius ρ for various χ_0 's, with $\dot{K}_I = 20 \text{ MPa}\sqrt{\text{m}}/\text{s}$ and $T = 400 \text{ K}$.

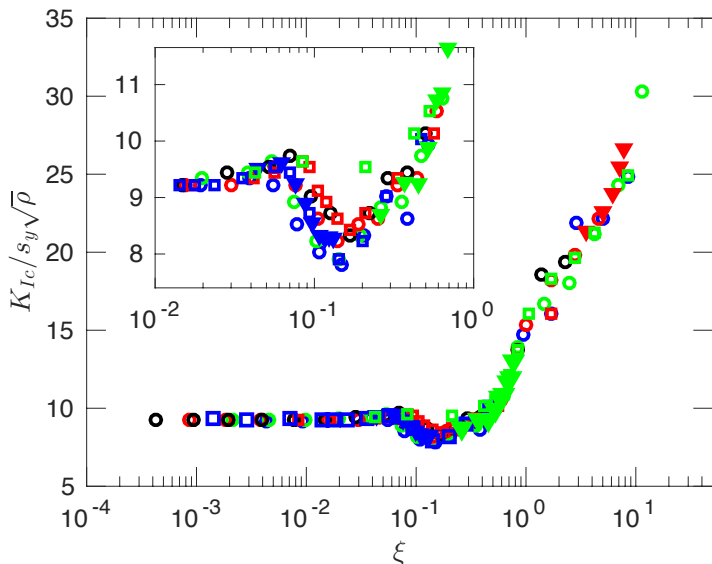


FIG. 5. (Color online) The dimensionless notch toughness $K_{Ic}(\chi_0, \dot{K}_I, \rho, T)/(s_y\sqrt{\rho})$ as a function of ξ , using all the data presented in Fig. 4. As predicted theoretically in Eq. (15), all data sets (except one in the non-monotonic part of the curve) collapse on a single master curve being a constant for $\xi \ll 1$, varying as $\log(\xi)$ for $\xi \gg 1$ and featuring a non-monotonic behavior for $\xi \sim \mathcal{O}(1)$. (inset) Zooming in on the non-monotonic part of the toughness master curve. Note in particular that data corresponding to the monotonic variation of the toughness with ρ in Fig. 4c nicely collapse on the non-monotonic part of the master curve (filled triangles) and that one data set (open green squares) do not exhibit a non-monotonic behavior (corresponding to the $\chi_0 = 640 \text{ K}$ data set in Fig. 4a).

prediction, we re-plot in Fig. 5 the data appearing in Fig. 4 as $K_{Ic}/s_y\sqrt{\rho}$ vs. ξ in linear-log scale. We observe that as predicted, all data collapse onto a single master curve in the $\xi \ll 1$ limit, where it is a constant, and in

the $\xi \gg 1$ limit, where it varies as $\log(\xi)$, and feature a *non-monotonic* behavior for $\xi \sim \mathcal{O}(1)$ for a broad range of parameters.

Note in particular the data corresponding to variations in ρ , which fall onto the non-monotonic parts of the curve and on the $\log(\xi)$ part. That means that while K_{Ic} is monotonic in ρ , when the proper dimensionless variables are used, it can reveal the non-monotonic behavior of the toughness master curve. Furthermore, it implies that the dependence of K_{Ic} on ρ differs from the existing literature, both theoretical and experimental, where K_{Ic} is expected to be either proportional to or linear in $\sqrt{\rho}$, mainly based on dimensional arguments [23, 26, 27, 29, 30, 34]. While this dependence would give *apparently* reasonable fits to the data in Fig. 4c, our analysis shows that there exists an *additional* and previously overlooked dependence on ρ through $\xi(\chi_0, \dot{K}_I, \rho)$, for both $\xi \sim \mathcal{O}(1)$ and $\xi \gg 1$.

It should be stressed that the crossover from the $\xi \ll 1$ behavior to the $\xi \gg 1$ behavior, with the possible non-monotonicity, is directly related to the change in the transition rate factor \mathcal{C} in Eq. (5) with increasing stress, from thermal activation at relatively small stresses to athermal processes at higher stresses. This change in behavior, which is not commonly discussed in the literature, implies that different parts of the function $K_{Ic}(\chi_0, \dot{K}_I, \rho, T)$ will depend differently on the temperature (note, though, that we have not considered other possible dependencies on the temperature). In particular, we have verified that the $\log(\xi)$ dependence originates from thermal activation (e.g. it disappears if thermal activation is eliminated altogether and its logarithmic slope varies in proportion to T), which suggests that glasses exhibit appreciable thermal effects well below their glass temperature. These predictions can be tested by systematically performing notch toughness experiments at different temperatures.

Figure 5, which summarizes our main result, provides a comprehensive picture of the notch toughness of glasses

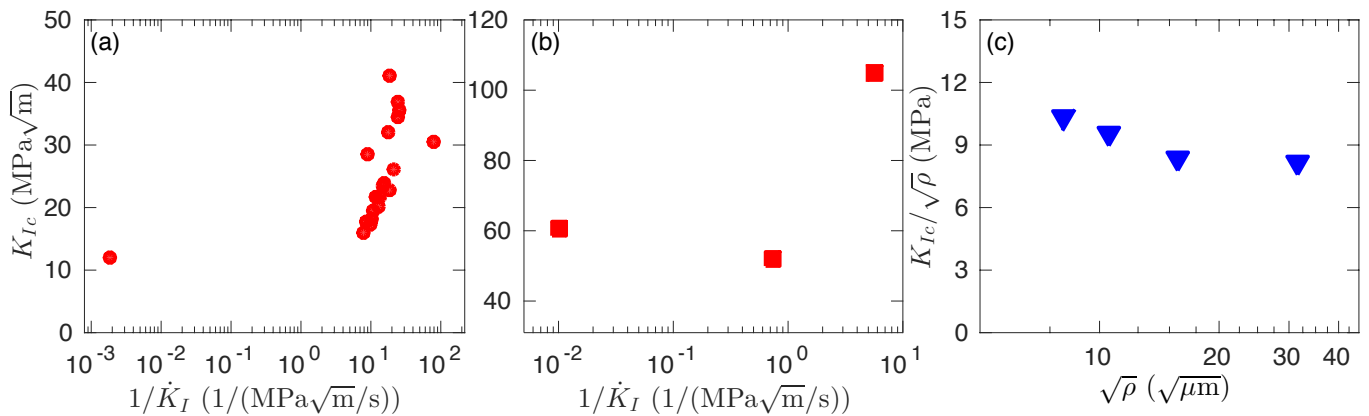


FIG. 6. (Color online) Experimental support for Bulk Metallic Glasses (BMG). (a) The notch fracture toughness data $K_{Ic}(\dot{K}_I)$ of [25] re-plotted as K_{Ic} vs. $\log(1/\dot{K}_I)$, following the theoretical prediction in Eq. (15). (b) The same as panel (a), but for the data of [26]. (c) The notch fracture toughness data $K_{Ic}(\rho)$ of [27] re-plotted as $K_{Ic}/\sqrt{\rho}$ vs. $\log(\sqrt{\rho})$, following the theoretical prediction in Eq. (15).

and various testable predictions. It shows that the toughness emerges from a competition between the *initial* (*i.e. far from steady-state*) plastic relaxation timescale, which depends on the glass history/age, and an effective loading timescale near the notch root, which depends on the global problem through \dot{K}_I and on the notch geometry through ρ . It also shows that the notch fracture toughness of glasses can vary quite substantially, as was claimed in [33], by changing ξ . The toughness shown in Figs. 4-5 implies a variation of more than an order of magnitude in the fracture energy $\Gamma \propto K_{Ic}^2/\mu$ [1].

V. EXPERIMENTAL EVIDENCE

While the toughness of glasses was experimentally studied by various groups, there are relatively few works that systematically vary the stress-intensity-factor rate, the age of the glass and the notch radius over a large range. In Fig. 6 we show three experimental data sets for BMG available in the literature, where the notch toughness was measured as a function of \dot{K}_I (panels (a) and (b)) and ρ (panel (c)).

Inspired by the theoretical prediction in Eq. (15) and its numerical validation in Fig. 5, we re-plot in Fig. 6a-b the data of [25] and of [26], respectively, as K_{Ic} vs. $\log(1/\dot{K}_I)$. The data in panel (a) are consistent with our predictions as they feature a quasi-logarithmic dependence on $\log(1/\dot{K}_I)$ for small \dot{K}_I and indicate the existence of a plateau for large \dot{K}_I 's. There is, however, a gap of nearly 4 orders in magnitude in \dot{K}_I in the data, so the possible non-monotonic behavior at intermediate \dot{K}_I 's cannot be tested. The data on panel (b) feature all of the predicted trends, including a non-monotonicity of a similar magnitude compared to our prediction, though there are too few experimental points to test functional dependencies.

In Fig. 6c we re-plot the data of [27] as $K_{Ic}/\sqrt{\rho}$ vs. $\log(\sqrt{\rho})$. The experimental data, where ρ ranges from 65 μm to 250 μm , seem to be consistent with the decreasing part of the toughness master curve in Fig. 5 and possibly indicate the existence of a minimum. A broader range of ρ 's, together with varying also χ_0 and \dot{K}_I , are needed in order to test the predicted functional dependencies, but it is already clear that re-plotting the existing data inspired by to our theory reveals new features of the toughness. Our theory certainly calls for additional experiments, as it offers various new qualitative and quantitative predictions.

VI. CONCLUDING REMARKS AND PROSPECTS

In this paper we provided a comprehensive theory of the notch fracture toughness of glassy solids, focussing on its dependence on the structural state of the glass (quantified by the initial value of the effective disorder temperature χ_0), on the stress-intensity-factor rate \dot{K}_I , on the notch radius of curvature ρ and on the temperature T below the glass transition temperature. The main results are the theoretical prediction in Eq. (15) and its numerical validation in Fig. 5 based on a novel computational method [48]. The theory highlights the underlying competition between an intrinsic plastic relaxation timescale and an extrinsic driving timescale, as well as the roles played by nonlinear yielding dynamics and a crossover between thermal/athermal rheological processes. The theoretical predictions are shown to be consistent with existing experimental data.

The analysis presented has been based on a simple version of the non-equilibrium thermodynamic Shear-Transformation-Zones (STZ) model [33]. We suspect that despite its relative simplicity, the model captures some salient features of glassy rheology, accounting for

generic properties of the notch fracture toughness of glasses. More elaborate models and quantitative predictions will be explored in the future. Other physical effects that were already identified in our numerical solutions, such as the time evolution of the notch curvature $\rho(t)$ and the propagation of plastic yielding fronts, will be reported on in a subsequent publication, along with discussing the post-cavitation dynamics. The latter were shown in [33] to lead to catastrophic failure, as we assumed in this work, though we did not discuss them at all.

A few important directions for future investigations emerge from the present analysis. Most notably, one would be interested in calculating the *intrinsic* toughness, as opposed to the notch toughness, in the limit of $\rho \rightarrow 0$, where the notch/tip radius of curvature is not the dominant lengthscale in the problem. This touches upon a fundamental problem in glass physics, i.e. the

existence on an intrinsic glassy lengthscale. Within the adopted non-equilibrium thermodynamic framework, such a lengthscale may appear in the macroscopic theory in an effective diffusion term proportional to $\nabla^2\chi$ in Eq. (4) [53, 63]. This will be discussed in separate report. Finally, it would be interesting to see whether variations in the glass composition, and their effect of the toughness, can be incorporated into the proposed theoretical framework.

Acknowledgments E.B. acknowledges support from the Israel Science Foundation (Grant No. 712/12), the Harold Perlman Family Foundation and the William Z. and Eda Bess Novick Young Scientist Fund. C.H.R. was supported by the National Science Foundation under Grant No. DMR-1409560, and by the Director, Office of Science, Computational and Technology Research, U.S. Department of Energy under contract number DE-AC02-05CH11231.

-
- [1] M.A Meyers and K.K. Chawla, *Mechanical Behavior of Materials*, (Cambridge University Press, Cambridge, 2009).
- [2] J.J. Gilman, *Mechanical behavior of metallic glasses*, J. Appl. Phys. **46**, 1625 (1975).
- [3] C.A. Schuh, T.C. Hufnagel and U. Ramamurthy, *Mechanical behavior of amorphous alloys*, Acta Mater. **55**, 4067 (2007).
- [4] M. Chen, *Mechanical behavior of metallic glasses: Microscopic understanding of strength and ductility*, Annu. Rev. Mater. Res. **38**, 445 (2008).
- [5] M.M. Trexler and N.N. Thadhani, *Mechanical properties of bulk metallic glasses*, Prog. Mater. Sci. **55**, 759 (2010).
- [6] Y.Q. Cheng and E. Ma, *Atomic-level structure and structure-property relationship in metallic glasses*, Prog. Mat. Sci. **56**, 379 (2011).
- [7] W. H. Wang, *The elastic properties, elastic models and elastic perspectives of metallic glasses*, Prog. Mat. Sci. **57**, 487 (2012).
- [8] T. Egami, T. Iwashita and W. Dmowski, *Mechanical properties of metallic glasses*, Metals **3**, 77 (2013).
- [9] T.C. Hufnagel, C.A. Schuh and M.L. Falk, *Deformation of metallic glasses: Recent developments in theory, simulations, and experiments*, Acta Mater. (*In press*).
- [10] F. Spaepen, *A microscopic mechanism for steady state inhomogeneous flow in metallic glasses*, Acta Metall. **25**, 407 (1977).
- [11] A.S. Argon, *Plastic deformation in metallic glasses*, Acta Metall. **27**, 47 (1979).
- [12] M.L. Falk and J.S. Langer, *Dynamics of viscoplastic deformation in amorphous solids*, Phys. Rev. E **57**, 7192 (1998).
- [13] L.C.E. Struik, *Physical aging in amorphous polymers and other materials*, Elsevier: Amsterdam, (1978).
- [14] M.D. Ediger, C.A. Angell and S.R. Nagel, *Supercooled liquids and glasses*, J. Phys. Chem. **100**, 13200 (1996).
- [15] A.L. Greer, *Metallic glasses*, Science **267**, 1947 (1995).
- [16] A. Inoue, *Stabilization of metallic supercooled liquid and bulk amorphous alloys*, Acta Mater. **48**, 279 (2000).
- [17] W.L. Johnson, *Bulk amorphous metal – an emerging engineering material*, JOM **54**, 40 (2002).
- [18] J.F. Löffler, *Bulk Metallic Glasses*, Intermetallics **11**, 529 (2003).
- [19] W.H. Wang, C. Dong and C.H. Shek, *Bulk Metallic Glasses*, Mat. Sci. Engg. R **44**, 45 (2004).
- [20] M.F. Ashby and A.L. Greer, *Metallic glasses as structural materials*, Scri. Mater. **54**, 321 (2006).
- [21] J.J. Lewandowski, *Effects of annealing and changes in stress state on fracture toughness of bulk metallic glass*, Mater. Trans. JIM **42**, 633 (2001).
- [22] J.J. Lewandowski, W.H. Wang and A.L. Greer, *Intrinsic plasticity or brittleness of metallic glasses*, Phil. Mag. Lett. **85**, 77 (2005).
- [23] P. Lowhaphandu and J.J. Lewandowski, Scrip. Mater. **38**, 1811 (1998).
- [24] M.D. Demetriou, M.E. Laubey, G. Garrett, J.P. Schramm, D.C. Hofmann, W.L. Johnson and R.O. Ritchie, *A damage-tolerant glass*, Nat. Mater. **10**, 123 (2011).
- [25] K.M. Flores and R.H. Dauskardt, *Crack-tip plasticity in bulk metallic glasses*, Mater. Sci. Eng. **A319-321**, 511 (2001).
- [26] K. Fujita, A. Okamoto, N. Nishiyama, Y. Yokohama, H. Kimura and A. Inoue, *Effects of loading rates, notch root radius and specimen thickness on fracture toughness in bulk metallic glasses*, J. Alloys and Compounds, **434-435**, 22 (2007).
- [27] J.J. Lewandowski, M. Shazly and A. Shamimi Nouri, *Intrinsic and extrinsic toughening of metallic glasses*, Scri. Mater. **54**, 337 (2006).
- [28] P. Tandaiya, R. Narasimhan and U. Ramamurthy, *Mode I crack tip fields in amorphous materials with application to metallic glasses*, Acta Mater. **55**, 6541 (2007).
- [29] J. Xu, U. Ramamurthy and E. Ma, *The fracture toughness of bulk metallic glasses*, JOM **62**, 10 (2010).
- [30] D.L. Henan and L. Anand, *Fracture of metallic glasses at notches: Effects of notch-root radius and the ratio of the elastic shear modulus to the bulk modulus on toughness*, Acta Mater. **57**, 6057 (2009).
- [31] P. Tandaiya, U. Ramamurthy and R. Narasimhan, *Mixed*

- mode (I and II) crack tip fields in bulk metallic glasses, *J. Mech. Phys. Solids* **57**, 1880 (2009).
- [32] R. Narasimhan, H.Y. Subramanya, S.D. Patil, P. Tandaiya and U. Ramamurty, *Stationary crack tip fields in elastic-plastic solids: An overview of recent numerical simulations*, *J. Phys. D: Appl. Phys.* **42**, 214005 (2009).
- [33] C.H. Rycroft and E. Bouchbinder, *Fracture toughness of metallic glasses: Annealing-induced embrittlement*, *Phys. Rev. Lett.* **109**, 194301 (2012).
- [34] R. Narasimhan, P. Tandaiya, I. Singh, R. L. Narayan and U. Ramamurty, *Fracture in metallic glasses: Mechanics and mechanisms*, *Int. J. Fract.* **191**, 53 (2015).
- [35] B.A. Sun and W.H. Wang, *The fracture of bulk metallic glasses*, *Prog. Mater. Sci.* **74**, 211 (2015).
- [36] W. Li, Y. Gao and H. Bei, *On the correlation between microscopic structural heterogeneity and embrittlement behavior in metallic glasses*, *Sci. Rep.* **5**, 14786 (2015).
- [37] B. Ding, X. Li, X. Zhang, H. Wu, Z. Xu and H. Gao, *Brittle versus ductile fracture mechanism transition in amorphous lithiated silicon: From intrinsic nanoscale cavitation to shear banding*, *Nano Energy* **18**, 89 (2015).
- [38] K.M. Flores and R.H. Dauskardt, *Mean stress effects on flow localization and failure in a bulk metallic glass*, *Acta Mater.* **49**, 2527 (2001).
- [39] E. Bouchaud, D. Boivin, J.-L. Pouchou, D. Bonamy, B. Poon and G. Ravichandran, *Fracture through cavitation in a metallic glass*, *Europhys. Lett.* **83**, 66006 (2008).
- [40] M.Q. Jiang, Z. Ling, J.X. Meng and L.H. Dai, *Energy dissipation in fracture of bulk metallic glasses via inherent competition between local softening and quasi-cleavage*, *Phil. Mag.* **88**, 407 (2008).
- [41] E. Bouchbinder, T.S. Lo and I. Procaccia, *Dynamic failure in amorphous solids via a cavitation instability*, *Phys. Rev. E* **77**, 025101 (2008).
- [42] E. Bouchbinder, T.S. Lo, I. Procaccia and E. Shtilerman, *Stability of an expanding circular cavity and the failure of amorphous solids*, *Phys. Rev. E* **78**, 026124 (2008).
- [43] P. Murali, T.G. Guo, Y.W. Zhang, R. Narasimhan, Y. Li and H.J. Gao, *Atomic scale fluctuations govern brittle fracture and cavitation behavior in metallic glasses*, *Phys. Rev. Lett.* **107**, 215501 (2011).
- [44] Q. An, G. Garrett, K. Samwer, Y. Liu, S.V. Zybin, S. N. Luo, M.D. Demetriou, W.L. Johnson, and W.A. Goddard, *Atomistic characterization of stochastic cavitation of a binary metallic liquid under negative pressure*, *J. Phys. Chem. Lett.* **2**, 1320 (2011).
- [45] P. Guan, S. Lu, M.J.B. Spector, P.K. Valavala and M.L. Falk, *Cavitation in amorphous solids*, *Phys. Rev. Lett.* **110**, 185502 (2013).
- [46] I. Singh, T.F. Guo, R. Narasimhan and Y.W. Zhang, *Cavitation in brittle metallic glasses - Effects of stress state and distributed weak zones*, *Int. J. Solids Struct.* **51**, 4373 (2014).
- [47] R. Maaß, P. Birckigt, C. Borchers, K. Samwer and C.A. Volkert, *Long range stress fields and cavitation along a shear band in a metallic glass: The local origin of fracture*, *Acta Mater.* **98**, 94 (2015).
- [48] C.H. Rycroft, Y. Sui and E. Bouchbinder, *An Eulerian projection method for quasi-static elastoplasticity*, *J. Comp. Phys.* **300**, 136 (2015).
- [49] A similar idea has been first discussed in the context of annealing-induced ductile-to-brittle (embrittlement) transitions in [33] and later in the context of necking instabilities in soft glasses in D.M. Hoyle and S.M. Fielding, *Age-dependent modes of extensional necking instability in soft glassy materials*, *Phys. Rev. Lett.* **114**, 158301 (2015).
- [50] J.S. Langer, *Dynamics of shear-transformation zones in amorphous plasticity: Formulation in terms of an effective disorder temperature*, *Phys. Rev. E* **70**, 041502 (2004).
- [51] E. Bouchbinder, J.S. Langer and I. Procaccia, *Athermal shear-transformation theory of amorphous plastic deformation. I. Basic principles*, *Phys. Rev. E* **75**, 036107 (2007).
- [52] E. Bouchbinder, J.S. Langer and I. Procaccia, *Athermal shear-transformation-zone theory of amorphous plastic deformation. II. Analysis of simulated amorphous silicon*, *Phys. Rev. E* **75**, 036108 (2007).
- [53] M.L. Manning, J.S. Langer and J.M. Carlson, *Strain localization in a shear transformation zone model for amorphous solids*, *Phys. Rev. E* **76**, 056106 (2007).
- [54] J.S. Langer, *Shear-transformation-zone theory of plastic deformation near the glass transition*, *Phys. Rev. E* **77**, 021502 (2008).
- [55] E. Bouchbinder and J.S. Langer, *Nonequilibrium thermodynamics of driven amorphous materials. I. Internal degrees of freedom and volume deformation*, *Phys. Rev. E* **80**, 031131 (2009).
- [56] E. Bouchbinder and J.S. Langer, *Nonequilibrium thermodynamics of driven amorphous materials. II. Effective-temperature theory*, *Phys. Rev. E* **80**, 031132 (2009).
- [57] E. Bouchbinder and J.S. Langer, *Nonequilibrium thermodynamics of driven amorphous materials. III. Shear-transformation-zone plasticity*, *Phys. Rev. E* **80**, 031133 (2009).
- [58] M.L. Manning, E.G. Daub, J.S. Langer and J.M. Carlson, *Rate-dependent shear bands in a shear-transformation-zone model of amorphous solids*, *Phys. Rev. E* **79**, 016110 (2009).
- [59] M.L. Falk and J.S. Langer, *Deformation and failure of amorphous, solid-like materials*, *Ann. Rev. Cond. Matt. Phys.* **2**, 353 (2011).
- [60] E. Bouchbinder and J.S. Langer, *Linear response theory for hard and soft glassy materials*, *Phys. Rev. Lett.* **106**, 148301 (2011).
- [61] C.H. Rycroft and F. Gibou, *Simulations of a stretching bar using a plasticity model from the shear transformation zone theory*, *J. Comp. Phys.* **231**, 2155 (2012).
- [62] N. Perchikov and E. Bouchbinder, *Variable-amplitude oscillatory shear response of amorphous materials*, *Phys. Rev. E* **89**, 062307 (2014).
- [63] K. Kamrin and E. Bouchbinder, *Two-temperature continuum thermomechanics of deforming amorphous solids*, *J. Mech. Phys. Solids* **73**, 269 (2014).
- [64] K.B. Broberg, *Cracks and Fracture*, (Academic Press, San Diego, 1999).